PHYSICSAccess Research Paper
ISSN Online: 2756-3898, ISSN Print: 2714-500X https://doi.org/10.47514/phyaccess.2026.6.2.013

Integrated Aeromagnetic Structural Mapping and Magnetic Source Depth Estimation of the Kaduna Basement Complex, Northwestern Nigeria: Implications for Regional Tectonics and Mineral Exploration

Hussaini Abdulkareem[1, 2], Abdullahi N Khalid[2], Cyril G Afuwai[2], Isa Y Hassan[3], Abdulhadi Danlami[4], and Mustapha T Lawal[1]

[1] Department of Physics, Faculty of Physical Sciences, Kaduna State University, Kaduna State, Nigeria
[2] Department of Geophysics, Faculty of Physical Sciences, Kaduna State University, Kaduna State, Nigeria
[3] Department of Scientific and Industrial Research, National Research Institute for Chemical Technology, Zaria, Kaduna State, Nigeria
[4] Department of Physics with Electronics, Nuhu Bamalli Polytechnic, Zaria, Kaduna State, Nigeria

Corresponding E-mail: Abdulkareem.hussaini@kasu.edu.ng

Received 21-06-2026
Accepted for publication 27-08-2026
Published 04-09-2026

Abstract

This study presents an integrated aeromagnetic investigation of Kaduna State, northwestern Nigeria, to delineate subsurface structures and estimate magnetic source depths within the Nigerian Basement Complex. Twenty-one high-resolution aeromagnetic datasets were analyzed using Reduction-to-Equator (RTE), Horizontal Gradient Magnitude (HGM), Centre for Exploration Targeting (CET), Euler Deconvolution, and Source Parameter Imaging (SPI). RTE anomalies range from −121.893 to 68.977 nT, reflecting lithological contrasts and structural features. HGM and CET analyses reveal dominant NE–SW and NW–SE structural trends associated with Pan-African deformation. Euler deconvolution indicates that SI = 1 provides the most coherent solutions, with depths ranging from less than 250 m to greater than 750 m, predominantly between 250 and 500 m. SPI estimates source depths of approximately 85–790 m, with deeper sources concentrated in the northwestern, southeastern, and southern sectors. The spatial correspondence among HGM maxima, CET lineaments, Euler solutions, and SPI-derived depths delineates a fault-controlled structural network and identifies structurally favourable zones for further mineral exploration and ground geophysical investigation. The study demonstrates the effectiveness of integrated aeromagnetic techniques for regional structural mapping and mineral exploration targeting in Precambrian basement terrains.

Keywords: Aeromagnetic Data; Reduction-to-Equator; Structural Lineaments; Horizontal Gradient Magnitude; Centre for Exploration Targeting; Euler Deconvolution; Source Parameter Imaging; Kaduna Basement Complex; Mineral Exploration.

I. Introduction

Magnetic surveying has a wide range of applications, extending from small-scale engineering to archaeological investigations [1-2]. Over the past several decades, magnetic methods have become indispensable tools in mineral exploration because of their rapid data acquisition, cost-effectiveness, and ability to investigate large and inaccessible terrains [3]. Significant advances in aeromagnetic interpretation have been achieved through improved survey design, reduced flight-line spacing, lower terrain clearance, and sophisticated processing algorithms capable of enhancing subtle magnetic anomalies [4]. These developments have increased the effectiveness of aeromagnetic data in delineating geological contacts, faults, shear zones, intrusive bodies, and mineralized structures.

The interpretation of aeromagnetic anomaly data for accurate estimation of source depths and identification of structural features such as faults, folds, dykes, and contacts requires the application of established geophysical techniques combined with sound geological insight. Among these techniques is the Reduction-to-Equator (RTE) transformation, first introduced by [5] and refined by [6], which re-centers anomalies over their sources. The Horizontal Gradient Magnitude (HGM) method is useful for delineating linear features such as fault zones and dykes from potential-field data [7–9]. The Centre for Exploration Targeting (CET) approach, described by [10], employs a suite of algorithms for automatic structural delineation, enhancement, lineament detection, and structural complexity analysis. Additionally, Euler deconvolution [11] provides estimates of source depth, geometry, and broader structural trends, while Source Parameter Imaging (SPI), developed by [12–14], provides a robust means of determining depths to magnetic sources.

Despite numerous aeromagnetic investigations within the Nigerian Basement Complex, the regional structural architecture of Kaduna State remains inadequately constrained, particularly with respect to the spatial distribution of deep-seated faults, fracture systems, and their implications for mineral exploration. Consequently, this study integrates Reduction-to-Equator (RTE), Horizontal Gradient Magnitude (HGM), Centre for Exploration Targeting (CET), Euler Deconvolution, and Source Parameter Imaging (SPI) techniques to delineate subsurface structures and estimate depths to magnetic source bodies. The results provide new insights into the tectonic framework of Kaduna State and identify structurally favorable zones that may control hydrothermal fluid migration and mineralization [15–18].

A. Location and Geology of the Study Area

The study area extends between latitudes 9°02′N and 11°32′N and longitudes 6°11′E and 8°45′E, encompassing the entirety of Kaduna State in northwestern Nigeria. Geologically, Kaduna State lies within the northwestern sector of the Nigerian Basement Complex (Fig. 1). It shares boundaries with Katsina State to the north, Nasarawa State and the Federal Capital Territory to the south, Plateau and Bauchi States to the east, and Niger State to the west.

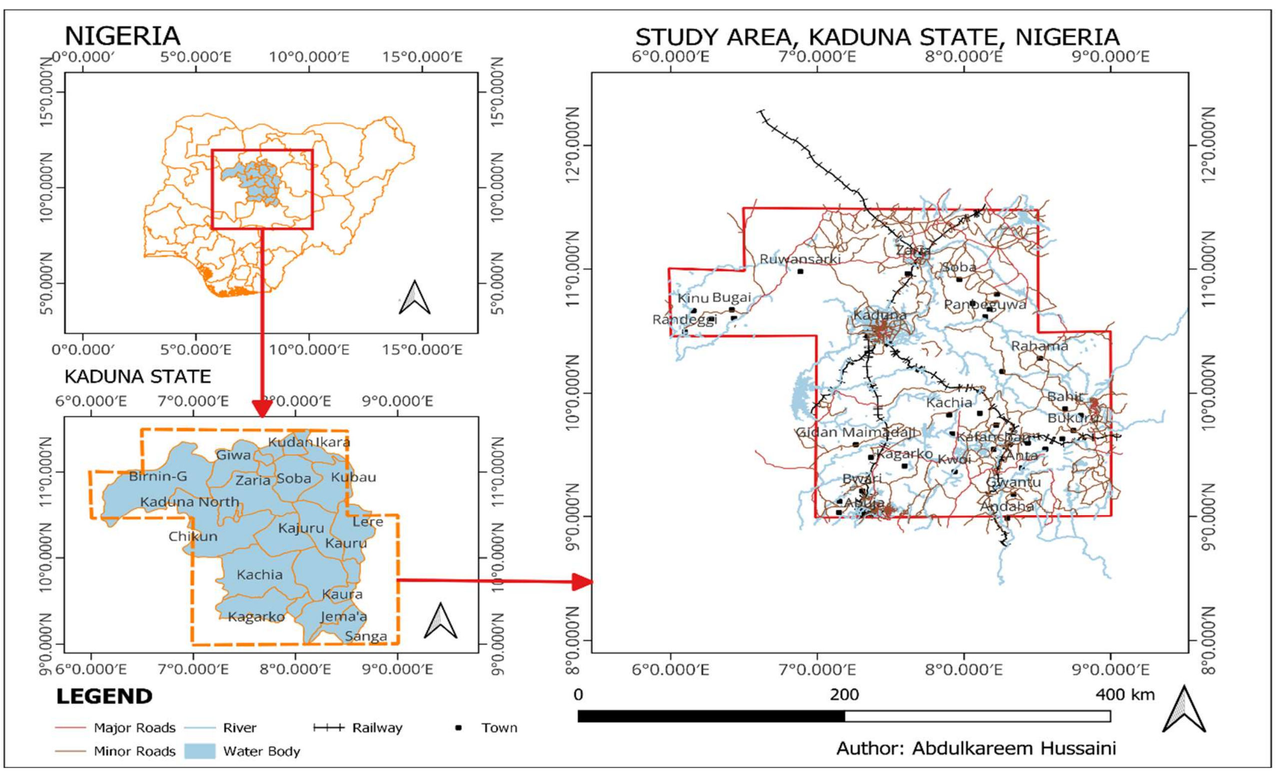

Fig. 1. Location map of the study area.

B. Geology of the Study Area

Kaduna State, situated in northwestern Nigeria, shares boundaries with Zamfara, Katsina, Kano, Bauchi, Niger, Nasarawa, and Plateau States, while its southwestern border adjoins the Federal Capital Territory (Abuja). The state covers an area of approximately 48,473.2 km², and lies within the northwestern Nigerian Basement Complex, underlain by a varied suite of Precambrian crystalline rocks that have experienced successive phases of deformation, metamorphism, and magmatic intrusion during the Pan-African Orogeny (Figs. 2 and 3). The region also contains Mesozoic and Tertiary intrusive and extrusive rocks. The Basement Complex, one of the three principal litho-petrological units of Nigeria, forms part of the Pan-African mobile belt, positioned between the West African and Congo Cratons and south of the Tuareg Shield [19]. Its lithology is predominantly composed of migmatites, granites, gneisses, schists, and quartzites.

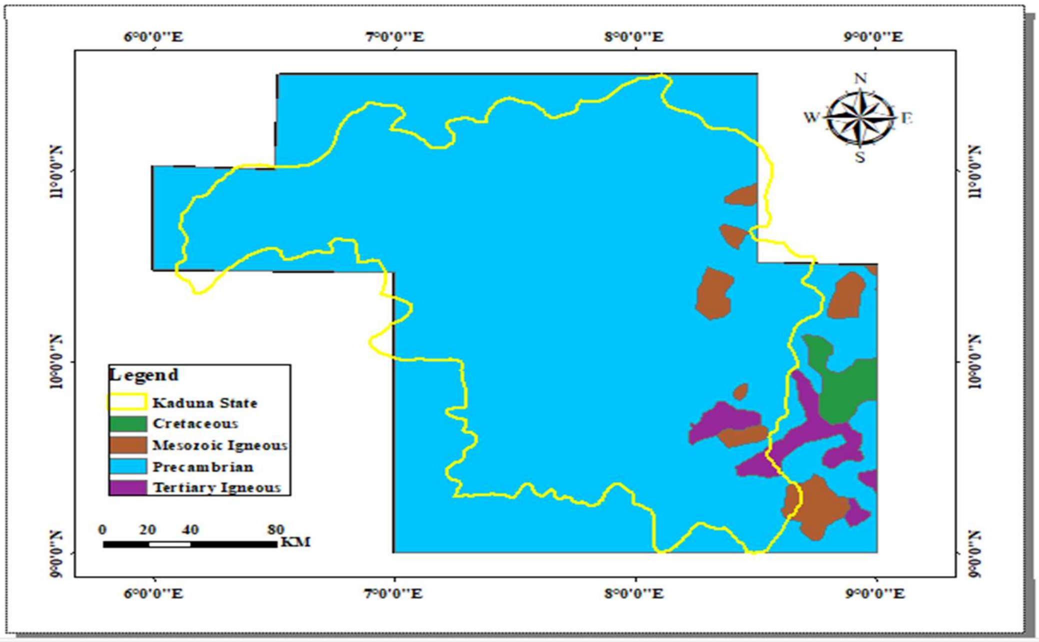

Fig. 2. Geological Map of the Study Area.

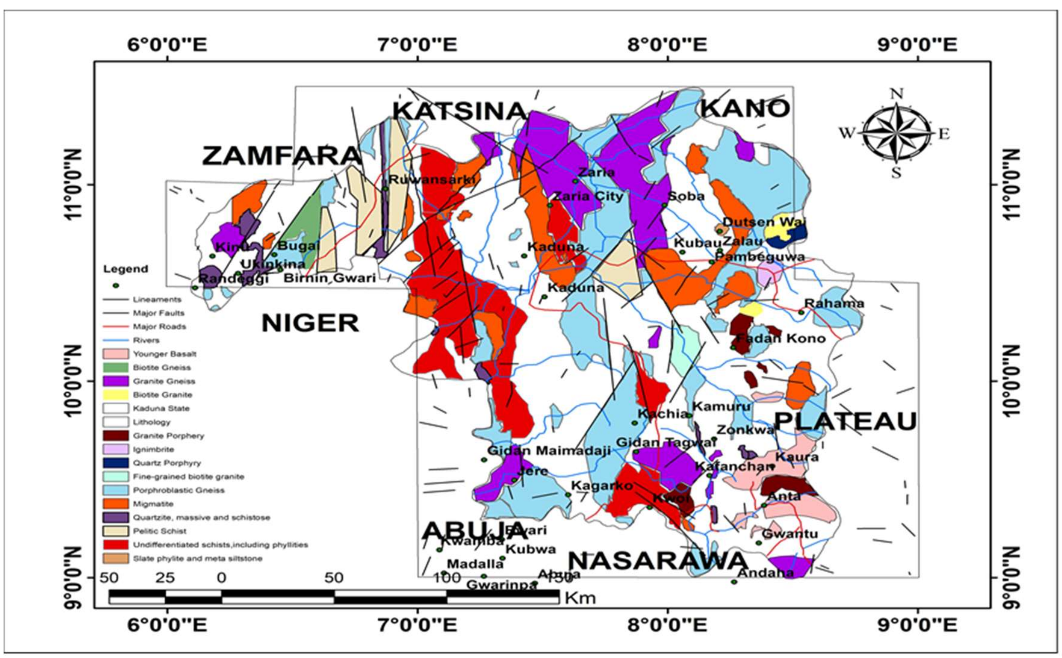

Fig. 3. Geological Map of the study area showing Lithology.

The Migmatite–Gneiss Complex, generally regarded as the basement complex, underlies the entire Kaduna State. It consists of migmatites, orthogneisses, paragneisses, and a suite of basic and ultrabasic metamorphosed rocks. Petrographic studies reveal that the Pan-African tectonothermal events induced extensive recrystallization of many constituent minerals through partial melting, with most rock types exhibiting medium- to upper-amphibolite-facies metamorphism [20].

The Schist Belts represent one of the most prominent structural features within the Basement Complex of Kaduna State. These belts predominantly trend in a NE–SW orientation and are particularly well developed in the western regions of Nigeria [21]. Historically, they were referred to as the "younger metasediments" to distinguish them from the migmatite–gneiss assemblages, which were classified as the "older metasediments."

Kaduna State hosts two principal schist belts: the Birnin-Gwari Schist Belt and the Kushaka Schist Belt. The Birnin-Gwari Belt is more extensive, stretching from Katsina State through Kaduna State and terminating near Minna in Niger State [22–23]. The dominant lithologies within this formation include phyllite, biotite–quartz–muscovite schist, and amphibolite schist. Both the Birnin-Gwari and Kushaka belts form part of the four recognized schist groups in Nigeria and are widely noted for their association with gold mineralization.

The Birnin-Gwari Schist Formation, together with the underlying quartzo-feldspathic rocks of the Zungeru Granulite Formation, constitutes a single structural unit known as the Zungeru–Birnin Gwari Schist Belt. This belt is expressed as a relatively simple north–south-trending syncline, approximately 150 km in length, with its northern segment offset dextrally by a NE–SW transcurrent fault [24]. The Birnin-Gwari Formation occupies the synclinal axis, with its lower sequence comprising finely banded phyllites in the west and higher-grade biotite–muscovite schists in the east. These are overlain by the Durimi pebbly schist, a metamorphosed mudstone conglomerate containing interbeds of impure quartzite and meta-greywacke. In contrast, the Kushaka Schist Formation is characterized by a series of curvilinear schist belts separated by gneissic domes and anticlines [25–26].

The lithology of the region is dominated by semi-pelitic biotite–muscovite schists, locally containing garnet and staurolite, with associated phyllites, metasiltstones, graphitic schists, and banded iron formations. Amphibolites and related schists reflect a tholeiitic basalt affinity, while to the east, a broad zone of migmatites and gneisses transitions into the Karaukarau Schist Belt, composed mainly of muscovite–biotite schists, phyllites, and quartzites. Minor graphitic and feldspathic schists, together with abundant quartz and quartz–tourmaline veins, highlight the complex metamorphic and structural evolution of the area.

The Karaukarau Schist Belt has been compared lithologically with the Kushaka Schist Belts [27–28], although notable differences exist. Unlike the chemically precipitated iron–silica formations of the Kushaka Belt, the quartzites in Karaukarau are detrital in origin, and rocks of basic igneous composition are far less significant. The succession represents a relatively well-differentiated sequence of mudstones and fine-grained sandstones. Structurally, the Karaukarau Belt closely resembles the Zungeru–Birnin Gwari Schist Belt, both in scale and geometry. Geochronological estimates indicate that the Karaukarau schists formed during the Pan-African Orogeny.

II. Materials and Methods

A. Aeromagnetic Data Acquisition and Processing

Twenty-one aeromagnetic sheets, namely Kuyambana (Sheet 100), Maska (Sheet 101), Zaria (Sheet 102), Ikara (Sheet 103), Sheet 121, Kushaka (Sheet 122), Kaduna (Sheet 123), Igabi (Sheet 124), Ditsenwai (Sheet 125), Kakuri (Sheet 144), Kajuru (Sheet 145), Geshere (Sheet 146), Lere (Sheet 147), Bishini (Sheet 165), Kachia (Sheet 166), Kafanchan (Sheet 167), Naraguta (Sheet 168), Abuja (Sheet 186), Gitata (Sheet 187), Jemaa (Sheet 188), and Kurra (Sheet 189), were used in this investigation. The aeromagnetic data were acquired from the Nigerian Geological Survey Agency (NGSA). The airborne survey was conducted by Fugro Airborne Surveys between 2005 and 2010 using three Scintrex CS3 cesium-vapour magnetometers mounted on a Cessna Caravan fixed-wing aircraft. Measurements were obtained at a nominal flight altitude of 100 m, corresponding to a mean terrain clearance of 80 m, along northwest–southeast-oriented flight lines spaced at 500 m intervals, with orthogonal tie lines spaced at 2000 m.

The datasets underwent standard preprocessing by Fugro Airborne Surveys and the NGSA. These procedures comprised positional corrections using differential Global Positioning System (DGPS), microlevelling, diurnal corrections, and removal of cultural magnetic noise associated with anthropogenic infrastructure, including power lines, pipelines, and communication facilities.

The twenty-one high-resolution aeromagnetic datasets were merged using Oasis Montaj (version 8.4) to produce a single continuous grid for the study area. The resulting grid was reprojected into the Universal Transverse Mercator (UTM) Zone 32N coordinate system to generate the Total Magnetic Intensity (TMI) map. Given the low magnetic latitude of the study area, Reduction to the Equator (RTE) was applied using a geomagnetic inclination of −2.8° and a declination of −1.69°. This transformation centres the magnetic anomalies over their causative sources, in accordance with standard practice for low-latitude regions. Regional trends were subsequently removed through trend filtering to obtain the Residual Magnetic Intensity (RMI) data.

B. Edge Detection and Depth Estimation of Magnetic Sources

Edge-detection techniques were applied to delineate structural features and identify buried subsurface anomalies. Several enhancement methods were applied to the aeromagnetic data, including Horizontal Gradient Magnitude (HGM), Source Parameter Imaging (SPI), and Euler Deconvolution analysis.

1) Horizontal Gradient Magnitude (HGM)

According to [29], the Horizontal Gradient Magnitude (HGM), also known as the total horizontal derivative, provides enhanced resolution and precision, particularly for datasets with wider line spacing. This technique is especially useful for delineating linear features such as fault zones and dykes from potential-field data [30]. The HGM of the potential-field anomaly was calculated as the Pythagorean sum of the horizontal gradients. For magnetic data, the HGM is given by

$$\text{HGM} = \sqrt{(\frac{\delta M}{\delta x})^2 + (\frac{\delta M}{\delta y})^2} \quad (1)$$

where $\frac{\delta M}{\delta x}$ and $\frac{\delta M}{\delta y}$ the terms represent the horizontal derivatives of the magnetic field in the x and y directions, respectively.

This function reaches its maxima over contacts and joints under the assumption that both the regional magnetic field and the magnetic sources are vertical, among other conditions. The ridges or maxima of the horizontal derivatives are widely regarded as reliable indicators of the edges of shallow, vertically dipping bodies. This enhancement is complementary to first vertical derivative techniques.

2) Centre for Exploration Targeting (CET) Grid

The Centre for Exploration Targeting (CET) Grid Analysis is an extension available in Geosoft Oasis Montaj that provides a suite of tools for analyzing image texture. These tools enable the automatic detection of lineaments along ridges, edges, and zones of structural complexity. The extracted lineaments are commonly interpreted as geological structures, particularly faults, which may be associated with potential mineralization in the study area.

Lineaments are typically extracted from the Reduction-to-the-Equator (RTE) map using the standard deviation method within the CET Grid Analysis workflow. Standard deviation is a statistical measure that quantifies local data variation at each grid location. Geological features of interest often exhibit significantly higher variability relative to the background signal. The standard deviation is calculated as given by (2).

$$\sigma = \sqrt{\frac{1}{N}\sum_{i=1}^{N}(x_i - \mu)^2} \quad (2)$$

where N is the number of cells in the window, μ is the average value, and x_i represents the cell values.

Lineament detection and construction of the associated rose diagram were performed through a multistep statistical workflow (Figs. 9 and 10). First, textural analysis was carried out using the standard deviation filter at a grid-cell scale of 1 cell = 10 m. Lineation detection was then conducted using phase symmetry analysis, applying a smallest filter wavelength of 4 cells, 3 filter scales, and a symmetry robustness value of 5. Finally, lineation vectorization was performed using an amplitude-threshold approach with an output ridge width of 3 cells and a threshold value of 0.1. This was followed by skeletonization (line thinning), using a grid-cell scale of 1 cell = 10 m, exclusion of lines shorter than 60 cells, and skeleton-to-vector conversion with line-deviation segmentation, whereby segments exceeding 3-cell deviation were divided.

The resulting vectorized structural map, generated in Oasis Montaj, was exported as an Esri Shapefile (.shp). The file was subsequently imported into ArcMap version 10.8, where geometric attributes were assigned to each structure based on the X and Y coordinates of the line start and end points. The processed shapefile was then imported into RockWorks 17 to generate the final rose diagram (Fig. 10).

3) Source Parameter Imaging (SPI)

The Source Parameter Imaging (SPI) technique is based on the relationship between source depth and the local wavenumber (K) of the analytic signal of the observed field [31].

The analytical signal $A_1(x, z)$ is given as in (3).

$$A_1(x, z) = \frac{\partial T(x,z)}{\partial x} - j\frac{\partial T(x,z)}{\partial z} \quad (3)$$

where $T(x, z)$ is the magnitude of the anomalous total magnetic field, j is an imaginary number, and x and z are Cartesian coordinates representing the vertical and horizontal directions, respectively, perpendicular to strike.

The local wavenumber k_1 is defined as in (4).

$$k_1 = \frac{\partial}{\partial x}\tan^{-1}\left(\frac{\partial T}{\partial z}\right)\Big/\left(\frac{\partial T}{\partial x}\right) \quad (4)$$

The analytical signal can also be defined based on the second-order derivatives, $A_2(x, z)$, such that

$$A_2(x, z) = \frac{\partial^2 T(x,z)}{\partial z \partial x} - j\frac{\partial^2 T(x,z)}{\partial^2 z} \quad (5)$$

Equation (5) gives rise to a second-order wavenumber, k_2, defined as

$$k_2 = \frac{\partial}{\partial x}\tan^{-1}\left(\frac{\partial^2 T}{\partial^2 z}\right)\Big/\left(\frac{\partial^2 T}{\partial x \partial z}\right) \quad (6)$$

Hence, the SPI technique requires first- and second-order wavenumbers (k_1 and k_2) for good data quality. The SPI depth estimates from the local wavenumbers of the analytic signals are obtained using the first vertical derivatives and horizontal gradients through Oasis Montaj software [32].

4) Euler Deconvolution

Euler Deconvolution is a three-dimensional semi-automatic interpretation technique that is primarily used for depth estimation and delineation of a wide variety of geological structures. It is based on the Euler homogeneity equation, which relates the magnetic field and its gradient components to the location of anomaly sources through the degree of homogeneity, N, referred to as the structural index (SI). The technique applies to geological structures such as contacts, faults, dykes, and sills and is calculated using (7).

$$(X - X_0)\frac{\partial T}{\partial x} + (Y - Y_0)\frac{\partial T}{\partial Y} + (Z - Z_0)\frac{\partial T}{\partial z} = N(B - T) \quad (7)$$

where (x_0, y_0, z_0) are the positions of the magnetic source; the total field T is observed at (x, y, z), B is the regional value (background value) of the total field, N is the structural index (SI), and the gradients represent the first derivatives in the x, y, and z directions.

An important parameter in the Euler equation is the structural index (N), which is a homogeneity factor relating the magnetic field and its gradient components to the location of the source [33–34]. The analysis was performed using the following parameters: a grid-cell size of 125, minimum-curvature interpolation, a residual filter with a trend surface and polynomial order of 1, and an Euler window size of 16.

III. Results and Discussion

The observed magnetic anomalies reflect significant lithological contrasts and structural discontinuities within the basement complex. Regions characterized by elevated magnetic amplitudes are interpreted as zones containing magnetite-rich granitoids, amphibolites, or mafic intrusions, whereas magnetic lows are attributed to weathered, altered, or fractured basement rocks with reduced magnetic susceptibility.

A. Total Magnetic Intensity (TMI) and Residual Magnetic Intensity (RMI)

The Total Magnetic Intensity (TMI) map (Fig. 4) exhibits pronounced magnetic highs and lows distributed throughout the study area, indicating substantial contrasts in magnetic susceptibility among the underlying lithological units. Magnetic highs are interpreted to be associated with magnetite-rich crystalline basement rocks, amphibolites, granitoids, and mafic intrusive bodies, whereas magnetic lows likely correspond to weathered basement rocks, altered zones, fractured terrains, and lithologies characterized by reduced ferromagnetic mineral content.

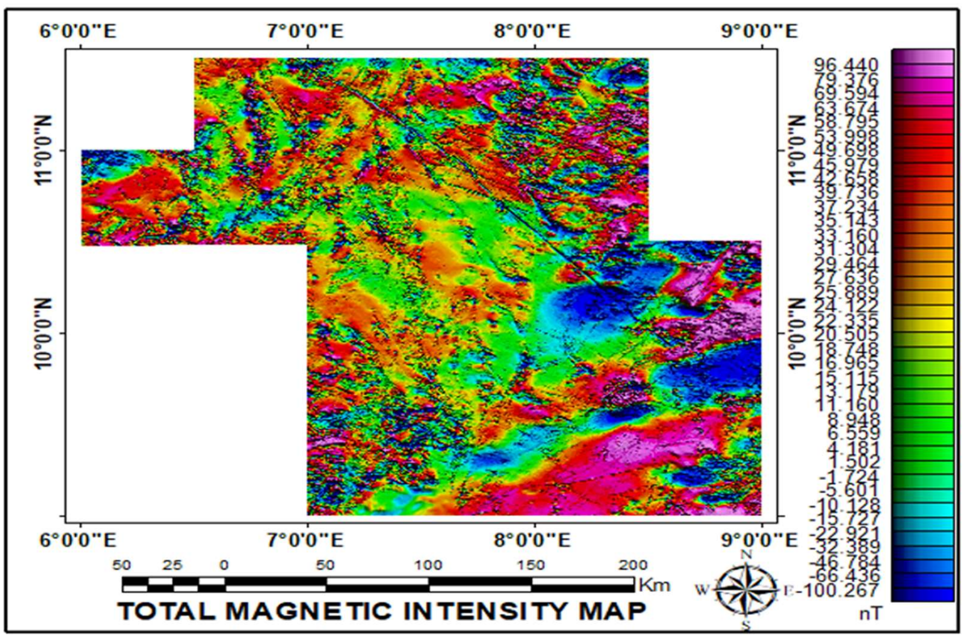

Fig. 4. Total magnetic intensity map.

The Residual Magnetic Intensity (RMI) map (Fig. 5) enhances local magnetic anomalies by removing long-wavelength regional components. The close similarity between the TMI and RMI maps suggests that the observed magnetic field is predominantly influenced by basement sources. The residual anomalies exhibit dominant NE–SW and NW–SE orientations, indicating the presence of multiple generations of tectonic deformation that have affected the basement rocks. The concentration of short-wavelength anomalies within the central and western portions of the study area is indicative of shallow magnetic sources, whereas broad, long-wavelength anomalies occurring within the northern and southern sectors suggest deeper magnetic bodies and regional structural controls.

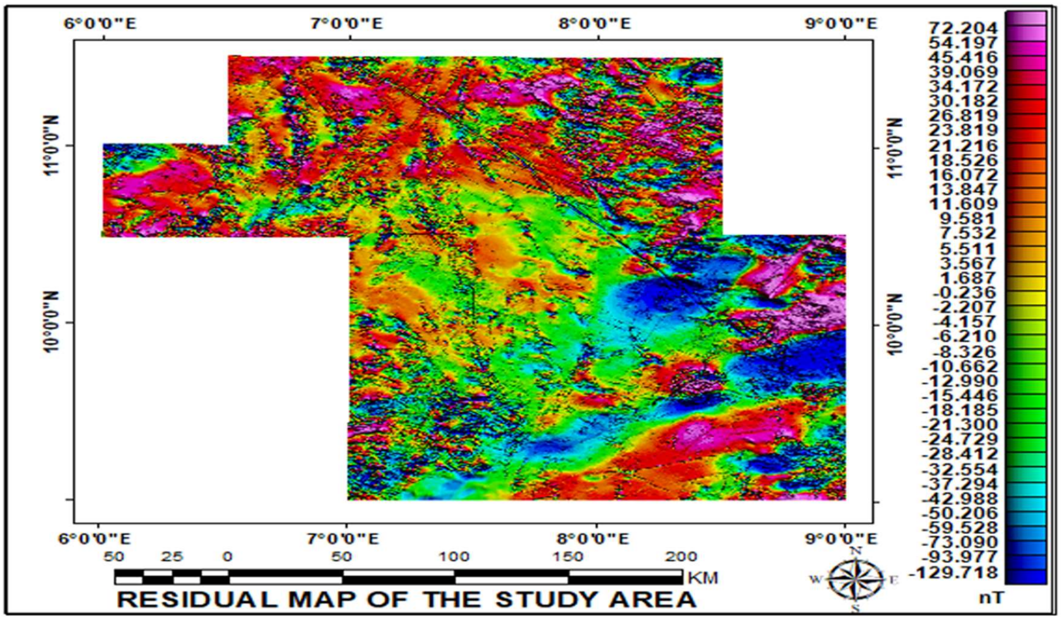

Fig. 5. Residual magnetic intensity map.

B. Regional Magnetic Intensity Map

A regional magnetic map represents broad, long-wavelength variations in the magnetic field associated with deep-seated geological structures. It depicts the regional magnetic field as the smooth, slowly varying component of the total magnetic field, which is influenced by deep crustal or mantle sources, including large igneous provinces, deep faults and shear zones, and basement-rock variations. It provides a framework for mapping deep faults and shear zones and for assessing the structure and composition of basement rocks beneath sedimentary cover [35–36]. The regional magnetic intensity map of the study area is depicted in Fig. 6. The dominant NE–SW and NW–SE structural trends visible on the residual-derived maps are largely filtered out, as expected. However, the regional magnetic high in the south coincides spatially with some of the deeper SPI sources, reinforcing the presence of deeper magnetic basement and structurally controlled blocks. These deep magnetic variations provide the regional framework within which shallower fault- and fracture-controlled features developed.

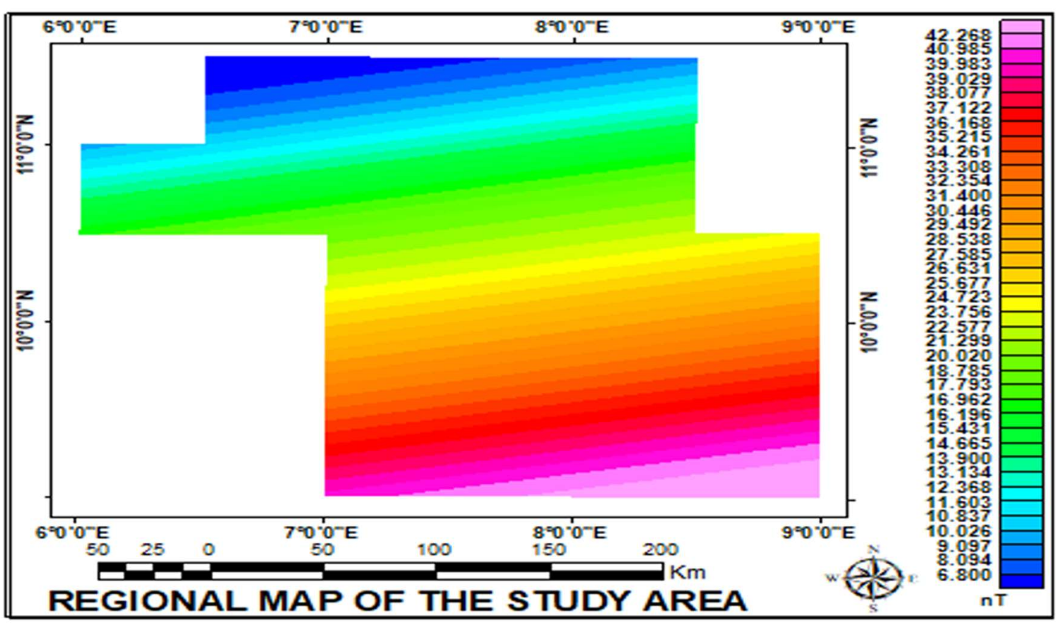

Fig. 6. Regional magnetic intensity map.

The southern magnetic high may indicate crustal domains that retained greater magnetic mineral content and could have supplied or channelled mineralizing fluids along reactivated Pan-African structures. Low-intensity zones indicate thick sedimentary covers or nonmagnetic lithologies overlying deeper basement structures, typical of subsided blocks or sedimentary basins. In contrast, high-intensity zones correspond to shallow igneous and metamorphic rocks, such as granites and gneisses, rich in magnetite. The magnetic pattern reveals a structural grain reflecting tectonic controls on lithological distribution and basement architecture. These features provide insights into subsurface geology, basement-depth variations, and potential targets for mineral exploration.

C. *Reduction-to-Equator (RTE) Interpretation*

Application of the Reduction-to-Equator (RTE) transformation significantly improved the spatial positioning of magnetic anomalies relative to their causative bodies [10]. The transformed anomalies exhibit enhanced symmetry and improved correlation with geological structures. The RTE map (Fig. 7) reveals several elongated magnetic features that trend predominantly NE–SW and NW–SE. These trends coincide with known regional structural orientations within the Nigerian Basement Complex and are interpreted as fault systems, shear zones, lithological contacts, and intrusive boundaries. The improved anomaly centring achieved through RTE processing facilitated subsequent structural interpretation using edge-detection techniques.

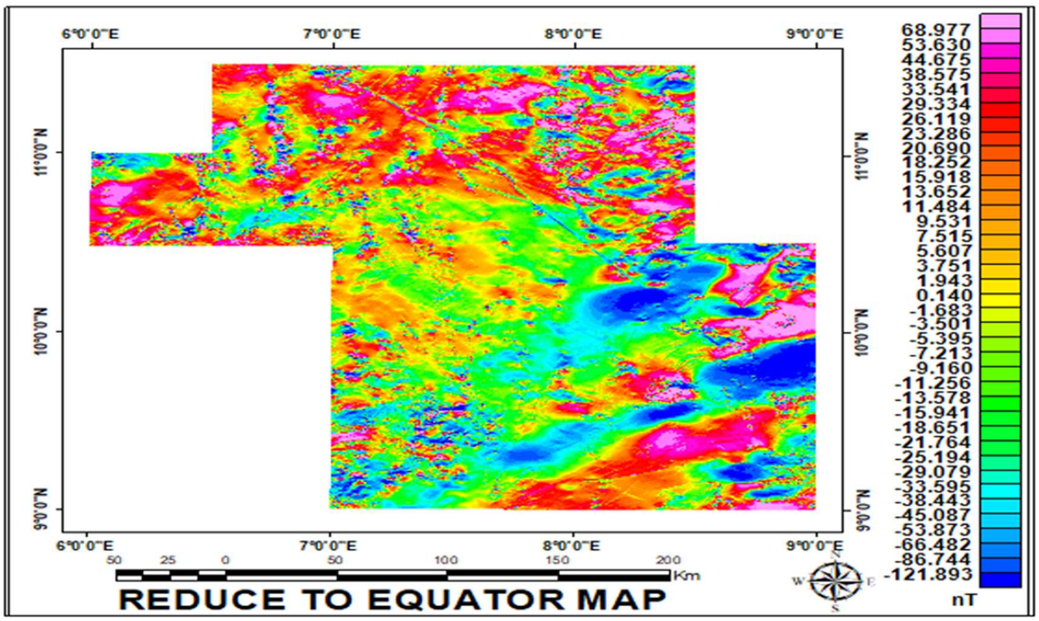

Fig. 7. Reduction-to-Equator map.

D. *Structural Delineation Using Horizontal Gradient Magnitude (HGM)*

The Horizontal Gradient Magnitude (HGM) map (Fig. 8) successfully delineates the boundaries of magnetic source bodies and highlights numerous structural discontinuities across the study area. High-gradient zones correspond to abrupt lateral changes in magnetic susceptibility and are interpreted as contacts, faults, fractures, dykes, and shear zones. The HGM analysis reveals two dominant structural orientations, NE–SW and NW–SE. These structural orientations are consistent with previously documented Pan-African tectonic fabrics within northwestern Nigeria and reflect multiple phases of crustal deformation. The NE–SW trend is particularly prominent and may represent reactivated basement structures that influenced fluid migration and mineralization processes.

E. *CET-Derived Lineament Analysis*

The Centre for Exploration Targeting (CET) analysis facilitated semi-automatic extraction of structural lineaments from the Reduction-to-the-Equator (RTE) magnetic data. The lineament map (Fig. 9) delineates a pervasive network of interconnected structural features across the study area. Concentrations of high lineament density are most prominent along NE–SW and NW–SE orientations, reflecting zones of pronounced structural complexity characterized by intense faulting and fracturing. These structurally active corridors are interpreted as domains of enhanced permeability that may be associated with hydrothermal fluid migration and potential control on mineralization. The intersections of major lineaments with favourable host lithologies or chemically reactive environments constitute structurally significant loci and represent priority targets for mineral exploration.

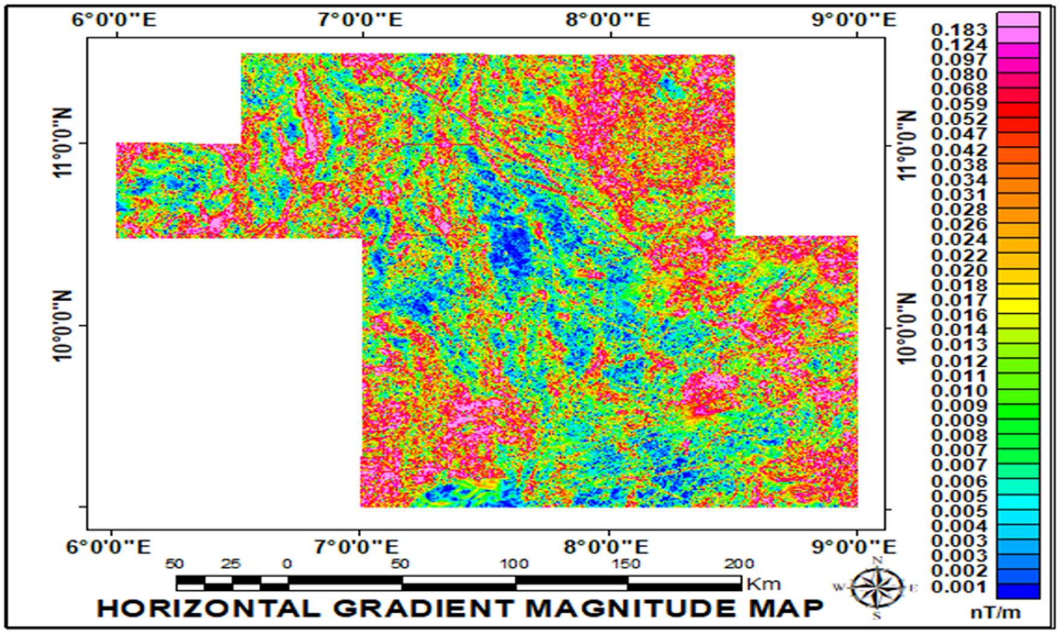

Fig. 8. Horizontal gradient magnitude map of the study area.

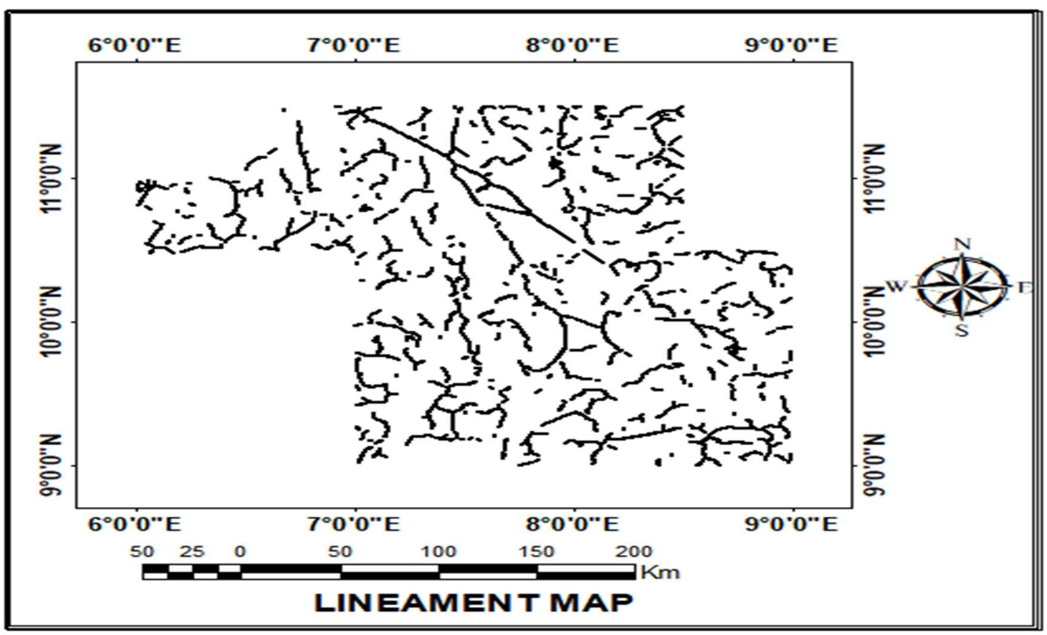

Fig. 9. Lineament map.

The rose diagram (Fig. 10) reveals a pronounced bimodal distribution of lineament orientations, with a dominant E–W/W–E trend reaching a peak frequency of approximately 252. This pronounced structural grain reflects anisotropy developed under an E–W/W–E principal stress regime and is interpreted as systematic joints, faults, or vein arrays formed during regional deformation. The high density and alignment of E–W/W–E fractures may have enhanced rock permeability and facilitated hydrothermal fluid migration, thereby suggesting prospective structural conditions for mineral exploration. Such structures may represent favourable targets for vein-type and structurally controlled mineralization where they intersect receptive host lithologies or chemical traps. Consequently, E–W/W–E structural corridors are regarded as priority targets for mineral exploration.

The lineament map superimposed on the Horizontal Gradient Magnitude map (Fig. 11) reveals marked spatial variations in structural intensity across the study area. Zones of high lineament density, shown in red to magenta, are concentrated in the NE–SW and NW–SE sectors and are interpreted as areas of intense fracturing and probable fault corridors. These structurally active corridors are interpreted as domains of enhanced permeability that may have facilitated hydrothermal fluid migration and may be associated with structurally controlled mineralization. In contrast, low-density areas, shown in blue and concentrated in the central and southern parts of the study area, correspond to more competent crustal blocks that experienced limited deformation. The overall distribution pattern accords well with the orientation statistics presented in the rose diagram (Fig. 10) and reinforces the structural framework derived from the geophysical data.

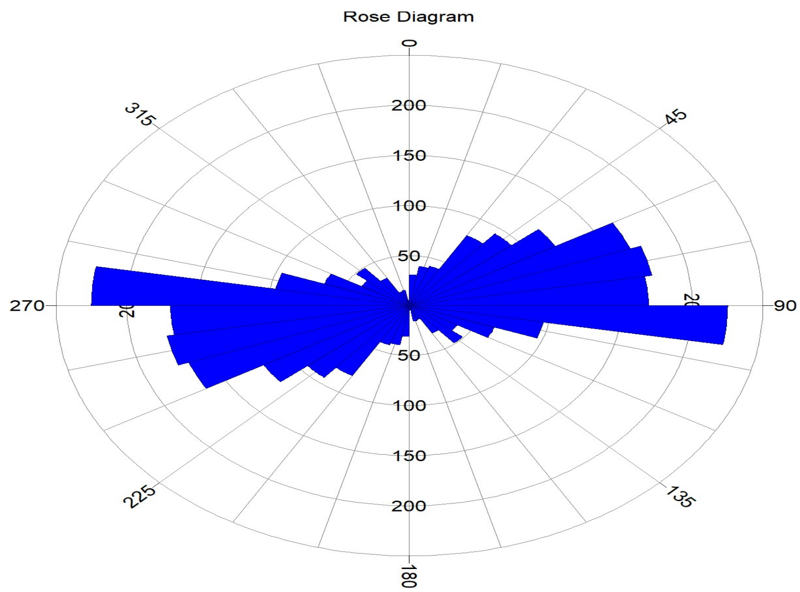

Fig. 10. Rose diagram.

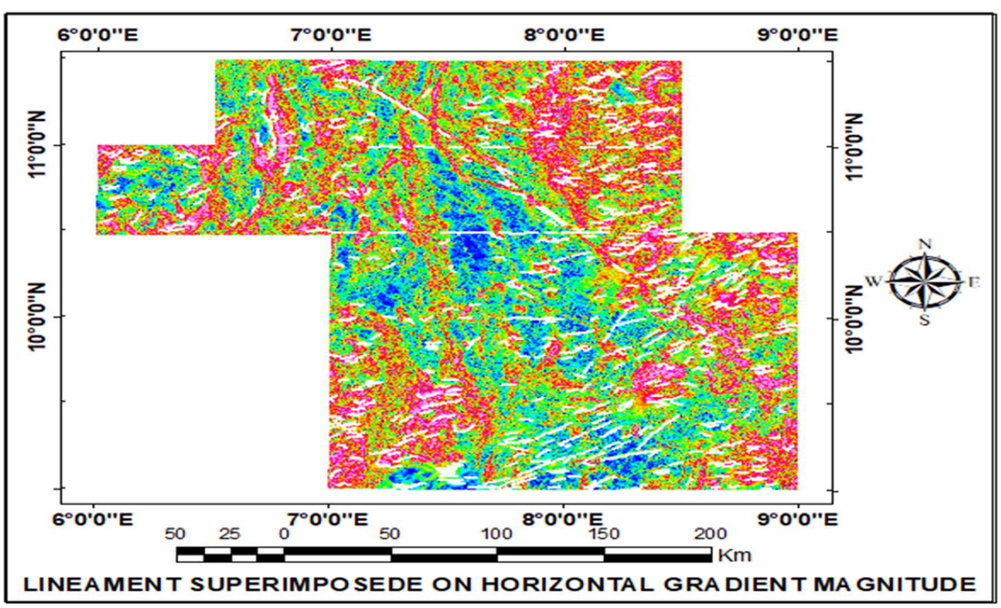

Fig. 11. Lineaments superimposed on the horizontal gradient magnitude map.

1) Implications for Mineral Exploration

The identified structural framework has important implications for mineral exploration within Kaduna State. Previous geological investigations have demonstrated that mineral deposits within the Nigerian Basement Complex are frequently structurally controlled and localized along major fault zones, shear zones, and fracture intersections. The lineament intersections identified in the present study represent potential zones of enhanced permeability that may have facilitated the migration and deposition of hydrothermal fluids. Such structural settings are particularly favourable for gold mineralization associated with the Birnin-Gwari and Kushaka Schist Belts. Consequently, areas characterized by high lineament density, structural intersections, and strong magnetic gradients are prioritized for detailed geological mapping, geochemical surveys, and ground geophysical investigations.

F. Source Parameter Imaging (SPI)

The Source Parameter Imaging (SPI) results (Fig. 12) provide quantitative estimates of magnetic source depths across the study area. Fig. 12 portrays a predominantly shallow-to-intermediate magnetic basement, mostly less than 500 m, across the study area, consistent with the thin residual cover typical of the Migmatite–Gneiss Complex. Localized deeper magnetic sources in the south and along the margins reflect fault-controlled basement topography inherited from Pan-African deformation. These deeper, structurally controlled zones, together with the dominant NE–SW and NW–SE lineament network, constitute prospective targets for further mineral exploration within the Precambrian basement terrain.

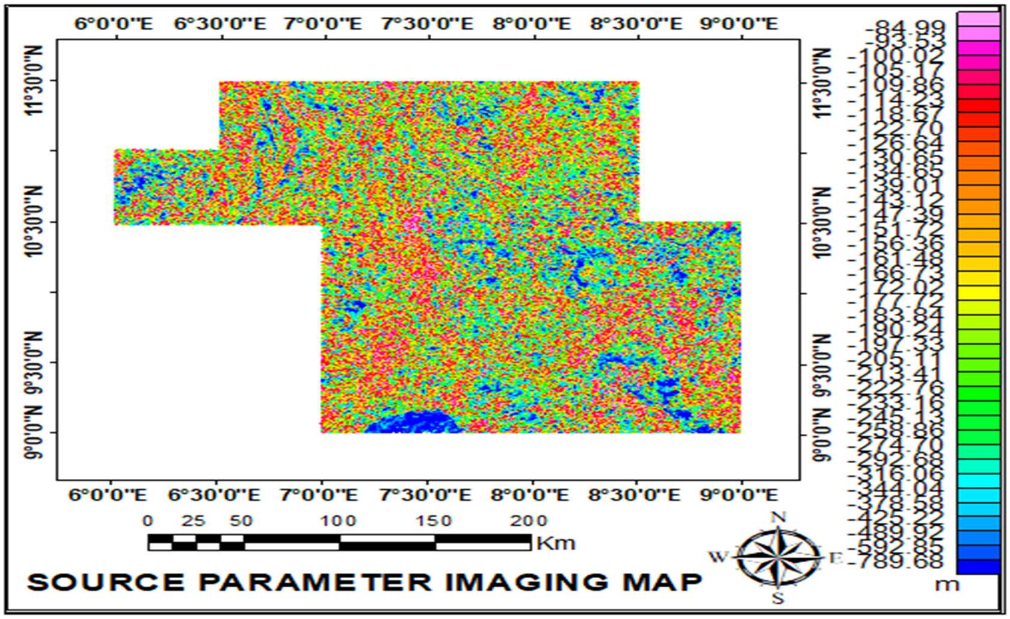

Fig. 12. Source Parameter Imaging map.

G. Euler Deconvolution Analysis

Euler deconvolution solutions generated using structural indices of 0, 1, 2, and 3 (Figs. 13–16) reveal significant variations in source geometry and depth distribution. Structural index 1 produced the most coherent clustering of solutions and the strongest spatial correspondence with geological structures identified from HGM and CET analyses. The SI = 1 solutions indicate that dyke-like, fault-controlled, and sill-related magnetic sources dominate the study area.

Most depth solutions fall between 250 and 500 m, although several deeper solutions exceed 750 m. The clustering of Euler solutions along major structural corridors suggests that fault systems represent the principal controls on the observed magnetic anomalies. The strong agreement between Euler depth solutions and HGM maxima confirms the effectiveness of integrating both methods for structural mapping and depth estimation.

Fig. 17 shows the Euler solutions (SI = 1) superimposed on the Horizontal Gradient Magnitude (HGM) map, which reveals strong spatial agreement with the high-anomaly zones.

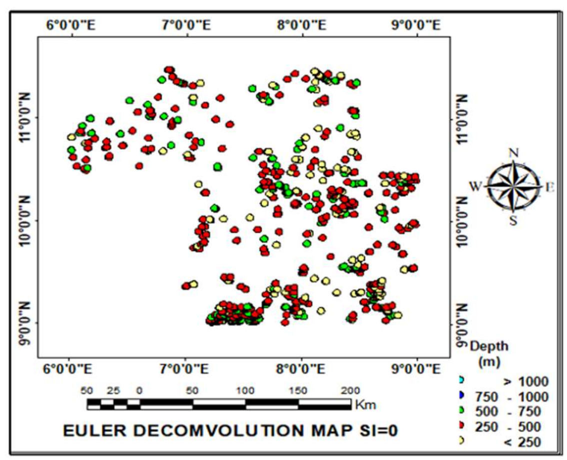

Fig. 13. Euler deconvolution (SI) = 0.

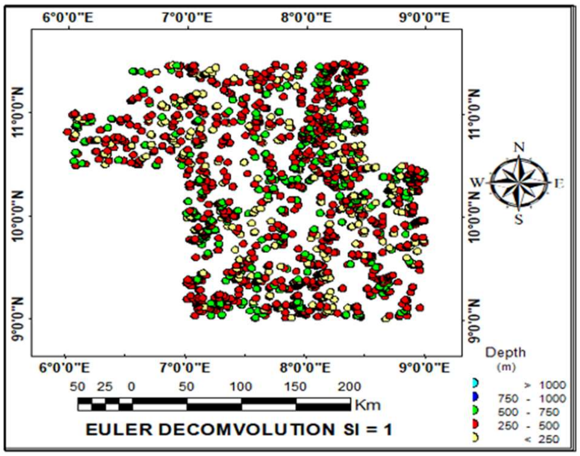

Fig. 14. Euler deconvolution (SI) = 1.

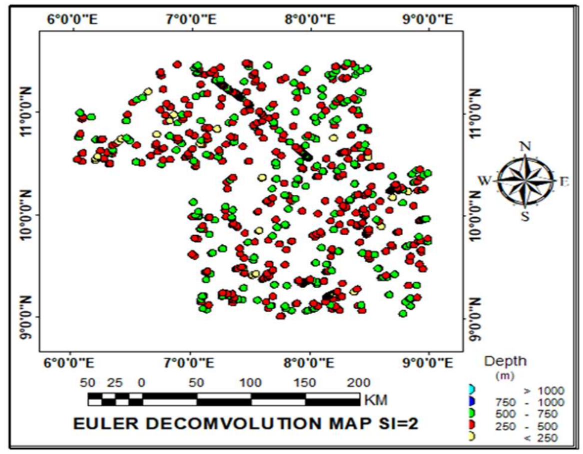

Fig. 15. Euler deconvolution (SI) = 2.

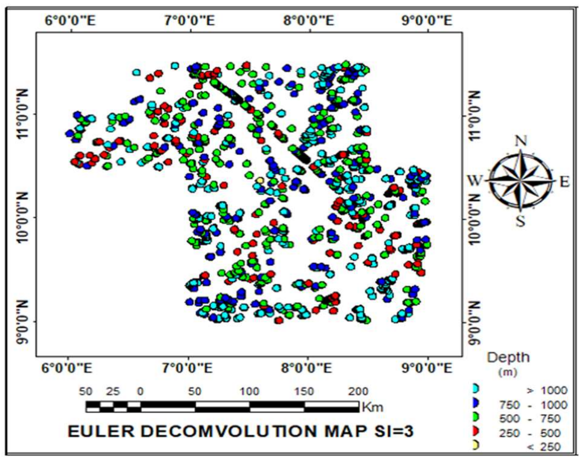

Fig. 16. Euler deconvolution (SI) = 3.

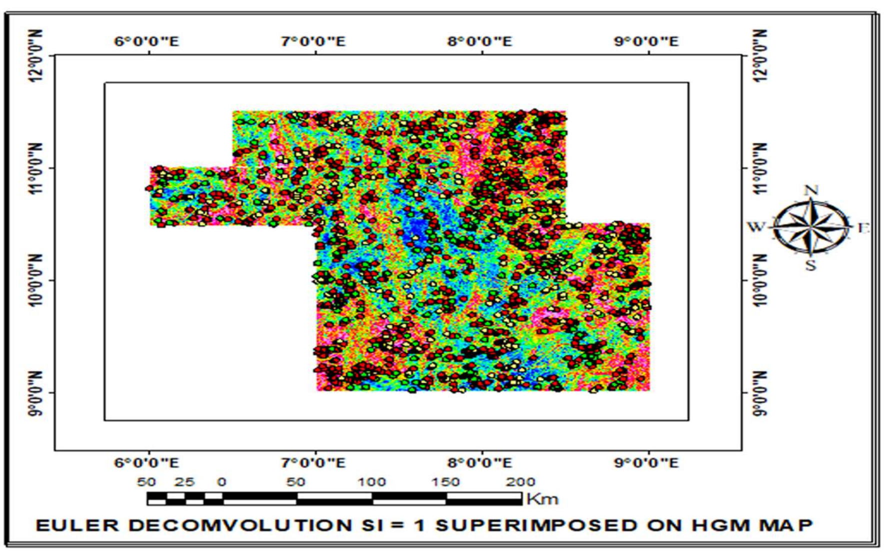

Fig. 17. Euler deconvolution with structural index (SI) = 1 superimposed on HGM MAP.

H. Discussion

The integrated interpretation of aeromagnetic data reveals a structurally complex basement terrain in Kaduna State, northwestern Nigeria, dominated by NE–SW and NW–SE-trending discontinuities, with subordinate NW–SE lineaments. These structural orientations are consistent with the regional tectonic grain of the Nigerian Basement Complex and are attributed to the Pan-African orogenic events that shaped the tectonic evolution of the region [37–38].

The spatial coincidence of HGM maxima, CET-derived lineaments, and Euler deconvolution clusters suggests the presence of significant faults and shear-zone structures. These tectonic structures have exerted a profound influence on the geological evolution and basement configuration of the study area, controlling both the emplacement and spatial distribution of lithological units. Spatial variations in magnetic signatures across the study area highlight contrasts in lithology, variations in the depth of magnetic sources, and differing intensities of structural deformation and basement modification.

The integration of TMI, RMI, RTE, HGM, SPI, and Euler techniques highlights a heterogeneous magnetic field characterized by alternating positive and negative anomalies. These patterns suggest strong tectonic control on the basement architecture, with NE–SW and E–W-trending anomalies reflecting the dominant structural grain. Negative magnetic anomalies are commonly associated with zones of intense fracturing, faulting, and hydrothermal alteration along shear zones, where magnetite is often altered to less magnetic phases.

This structural framework may be associated with mineralization in the region. The major faults and shear zones may have acted as conduits for mineralizing fluids, consistent with previous studies in Kaduna State and adjacent areas of northwestern Nigeria that link similar lineaments to gold and other mineral occurrences [39]. However, confirmation of mineralization within the identified structural zones requires further geological, geochemical, and ground-geophysical investigations.

IV. CONCLUSION

Structural analysis of the aeromagnetic data reveals prominent multidirectional high- and low-magnetic anomalies trending NE–SW and NW–SE across the study area. Significant structural trends are concentrated in the central region and reflect variations in lithology, magnetic susceptibility, strike, and depth. High-intensity zones on the Horizontal Gradient Magnitude (HGM) map coincide with lineaments obtained from CET Grid Analysis, indicating areas of significant magnetic and structural complexity that may constitute prospective targets for mineral exploration.

The Source Parameter Imaging (SPI) map delineates magnetic source depths, including edges, contacts, and faults, ranging from about 85 m for shallow sources to about 790 m for deeper sources. Accepted Euler deconvolution solutions (SI = 1) yield depths ranging from less than 250 m for shallow anomalies to approximately 750 m for deeper anomalies. These solutions exhibit strong spatial agreement with the high-anomaly zones of the HGM map.

The integrated interpretation reveals that the basement architecture of Kaduna State is complex and predominantly fault-controlled, with NE–SW and NW–SE trends constituting the dominant structural fabric. The observed spatial correlation among HGM maxima, CET-derived lineaments, Euler depth solutions, and SPI-derived source depths identifies multiple structurally favourable zones that constitute prospective targets for future mineral exploration and detailed ground-geophysical investigations.

References

[1] P. Kearey, M. Brooks, and I. Hill, An Introduction to Geophysical Exploration, 3rd ed. Great Britain: Blackwell Science Ltd., 2002.

[2] D. A. Clark, “Magnetic properties of rocks and minerals,” AGSO Journal of Australian Geology and Geophysics, vol. 17, no. 2, pp. 12–22, 1997.

[3] A. S. Murray and R. M. Tracey, Best Practice in Gravity Surveying. Canberra, Australia: Geoscience Australia, 2001.

[4] V. J. S. Grauch and P. S. Millegan, “Mapping intrabasinal faults from high-resolution aeromagnetic data,” The Leading Edge, vol. 17, no. 1, pp. 53–55, 1998.

[5] P. Gunn, “Airborne magnetic and radiometric survey,” AGSO Journal of Australian Geology and Geophysics, vol. 17, no. 2, p. 216, 1997.

[6] C. V. Reeves, S. W. Reford, and P. R. Milligan, “Airborne geophysics: Old methods, new images,” in Proc. Exploration 97: Fourth Decennial International Conference on Mineral Exploration, 1997, pp. 13–30.

[7] C. V. Reeves, “Continental scale and global geophysical anomaly mapping,” ITC Journal, vol. 2, pp. 91–98, 1998.

[8] P. R. Milligan and P. J. Gunn, “Enhancement and presentation of airborne geophysical data,” AGSO Journal of Australian Geology and Geophysics, vol. 17, no. 2, pp. 64–74, 1997.

[9] V. Baranov, “A new method of interpretation of aeromagnetic maps: Pseudo-gravimetric anomalies,” Geophysics, vol. 22, pp. 259–283, 1957.

[10] M. N. Rusman, S. Alawiyah, and I. Gunawan, “Study on the Significance of Reduction to the Equator (RTE), Reduction to the Pole (RTP), and Pseudogravity in Magnetic Data Interpretation,” Jurnal Penelitian Pendidikan IPA, vol. 9, no. 8, pp. 4705–4718, Aug. 2023. DOI: 10.29303/jppipa.v9i8.4705.

[11] J. D. Phillips, "Locating magnetic contacts: A comparison of the horizontal gradient, analytic signal and local wavenumber methods," in SEG Technical Program Expanded Abstracts, Calgary, AB, Canada, 2000, pp. 402–405.
[12] V. J. S. Grauch and L. Cordell, "Limitations of determining density or magnetic boundaries from the horizontal gradient of gravity or pseudo-gravity data," Geophysics, vol. 52, no. 1, pp. 118–121, 1987.
[13] E. J. Holden, M. Dentith, and P. Kovesi, "Towards the automated analysis of regional aeromagnetic data to identify regions prospective for gold deposits," Computers & Geosciences, vol. 34, no. 11, pp. 1505–1513, 2008, doi: 10.1016/j.cageo.2007.08.007.
[14] D. Core, A. Buckingham, and S. Belfield, "Detailed structural analysis of magnetic data—done quickly and objectively," SGEG Newsletter, vol. 1, no. 2, pp. 15–21, 2009.
[15] A. B. Reid et al., "Magnetic interpretation in three dimensions using Euler deconvolution," Geophysics, vol. 55, no. 1, pp. 80–91, 1990.
[16] J. B. Thurston and R. S. Smith, "Automatic conversion of magnetic data to depth, dip, and susceptibility contrast using the SPI method," Geophysics, vol. 62, no. 3, pp. 807–813, 1997.
[17] J. B. Thurston, J. C. Guillon, and R. S. Smith, "Model independent depth estimation with the SPI™ method," in SEG Technical Program Expanded Abstracts, 1999, pp. 403–406.
[18] J. B. Thurston, R. S. Smith, and J. C. Guillon, "A multi-model method for depth estimation from magnetic data," Geophysics, vol. 67, no. 2, pp. 555–561, 2002.
[19] E. Daniel, R. Jimoh, and K. Lawal, "Delineation of gold mineral potential zone using high-resolution aeromagnetic data over part of Kano State, Nigeria," Journal of Geology and Geophysics, vol. 8, no. 4, Art. no. 464, 2019, doi: 10.35248/2381-8719.464.
[20] J. Andrew, A. Alkali, K. A. Salako, and E. E. Udensi, "Delineating mineralization zones within the Keffi-Abuja area using aeromagnetic data," Journal of Geography, Environment and Earth Science International, vol. 15, no. 3, pp. 1–12, 2018, doi: 10.9734/JGEESI/2018/37052.
[21] O. B. Balogun, "Tectonic and structural analysis of the Migmatite–Gneiss–Quartzite Complex of Ilorin area from aeromagnetic data," NRIAG Journal of Astronomy and Geophysics, vol. 8, no. 1, pp. 22–33, 2019, doi: 10.1080/20909977.2019.1615795.
[22] O. I. Okwokwo, A. A. Adetona, T. Adewumi, and O. A. Sunday, "Interpretation of high-resolution aeromagnetic data to determine sedimentary thickness over part of Bida Basin, North Central Nigeria," Journal of Geology and Mining Research, vol. 10, no. 6, pp. 72–80, 2018, doi: 10.5897/JGMR2018.0293.
[23] M. N. Tijani, "Geology of Nigeria," in Landscapes and Landforms of Nigeria. Cham, Switzerland: Springer Nature Switzerland, 2023, pp. 3–32.
[24] S. S. Dada, O. Bruguier, N. G. Goki, I. A. Oha, M. A. O. Rahaman, and C. U. Ibe, "The Nigerian migmatite-gneiss complex: Product of Proterozoic reworking of a primitive crust," in Geology and Natural Resources of Nigeria, 1st ed. Boca Raton, FL, USA: CRC Press, 2024, pp. 29–39, doi: 10.1201/9781003454908-2.
[25] M. Lawal, M. A. Mohammed, K. A. Alalade, H. Hamidu, A. M. Shuaibu, N. A. Yelwa, Y. A. Omanayin, and F. S.-A. Adeniyi, "Geology of Basement Complex rocks in Kabo area, Kano, Northwestern Nigeria: Insights into the trends of mineralization in the region," International Journal of Scientific and Global Sustainability, vol. 11, no. 1, pp. 38–45, 2025, doi: 10.57233/ijsgs.v11i1.780.
[26] K. Oluyede, G. Ibrahim, U. Danbatta, P. Ogunleye, and U. Klötzli, "Field occurrence, petrography and structural characteristics of the Basement rocks in the northern part of Kushaka and Birnin Gwari schist belts, Northwestern Nigeria," Journal of Natural Sciences Research, vol. 12, no. 12, pp. 9–24, 2021, doi: 10.7176/JNSR/12-12-02.
[27] K. Oluyede, I. Garba, U. Danbatta, P. Ogunleye, and U. Klötzli, "Origin and geological setting of magmatic rocks within the Kushaka and Birnin Gwari Schist Belts, Northwest Nigeria," in Geology and Natural Resources of Nigeria, 1st ed. Boca Raton, FL, USA: CRC Press, 2024, ch. 8, doi: 10.1201/9781003454908-8.
[28] M. D. Tawey, D. U. Alhassan, A. A. Adetona, K. A. Salako, A. A. Rafiu, and E. E. Udensi, "Application of aeromagnetic data to assess the structures and solid mineral potentials in part of North Central Nigeria," Journal of Geography, Environment and Earth Science International, vol. 24, no. 5, pp. 11–29, 2020, doi: 10.9734/JGEESI/2020/v24i530223.
[29] S. P. Oliveira and L. T. Pham, "Stable calculation of horizontal derivatives of potential field data," Journal of Applied Geophysics, vol. 250, Art. no. 106223, 2026, doi: 10.1016/j.jappgeo.2026.106223.
[30] W. Lemotio, P. G. Kamto, L. T. Pham, F. E. K. Ghomsi, A. O. Ntouda, C. A. C. Fantah, N. Sévérin, and P. N. Nouck, "High-precision structural mapping using advanced enhancement methods of gravity anomalies in Southwest Cameroon (Central Africa): Tectonic implications," Acta Geophysica, vol. 72,

no. 4, pp. 2361–2375, 2024, doi: 10.1007/s11600-023-01223-0.
[31] O. S. Haruna, O. W. Osisanya, O. E. Agbalagba, A. I. Korode, and T. A. Ibitoye, "Application of aeromagnetic in determination of lineament of Hawal basement complex Northeast Nigeria," World News of Natural Sciences, vol. 45, pp. 58–92, 2022.
[32] A. B. Arogundade, M. O. Awoyemi, O. S. Hammed, S. C. Falade, and O. D. Ajama, "Structural investigation of Zungeru-Kalangai fault zone and its environ, Nigeria using aeromagnetic and remote sensing data," Heliyon, vol. 8, no. 3, Art. no. e09055, 2022, doi: 10.1016/j.heliyon.2022.e09055.
[33] D. C. Turner, "Upper Proterozoic schist belts in the Nigerian sector of the Pan-African province of West Africa," Precambrian Research, vol. 21, nos. 1–2, pp. 55–79, 1983.
[34] N. G. Obaje, "The basement complex," in Geology and Mineral Resources of Nigeria. Berlin, Germany: Springer, 2009, pp. 13–30.
[35] O. E. Eze et al., "Deciphering aeromagnetic data for sustainable sedimentary and structural insights in Obudu Plateau, Ikom Mamfe embayment and Oban Massif, southeastern Nigeria," Scientific Reports, vol. 15, Art. no. 40387, 2025, doi: 10.1038/s41598-025-24801-2.
[36] W. M. Telford, L. P. Geldart, and R. E. Sheriff, Applied Geophysics, 2nd ed. Cambridge, U.K.: Cambridge University Press, 1990.
[37] C. Reeves, Aeromagnetic Surveys: Principles, Practice and Interpretation. Geosoft, 2005.
[38] A. A. Adepoju, O. A. Akinlalu, and A. A. Adetona, "Exploration of iron ore deposits in parts of Kogi State, north-central Nigeria: Analyses from airborne magnetic and ASTER datasets," Geosystems and Geoenvironment, vol. 4, no. 2, Art. no. 100359, 2025, doi: 10.1016/j.geogeo.2025.100359.
[39] P. Stavrev and A. Reid, "Degrees of homogeneity of potential fields and structural indices of Euler deconvolution," Geophysics, vol. 72, no. 1, pp. L1–L12, 2007.